The role of shock waves in expansion tube accelerators

G. Olson, Richard Peterson, B. Pulford, M. Seaberg, K. Stein, C. Stelter, and R. Weber

Citation: American Journal of Physics **74**, 1071 (2006); doi: 10.1119/1.2366737
View online: http://dx.doi.org/10.1119/1.2366737
View Table of Contents: http://aapt.scitation.org/toc/ajp/74/12
Published by the American Association of Physics Teachers

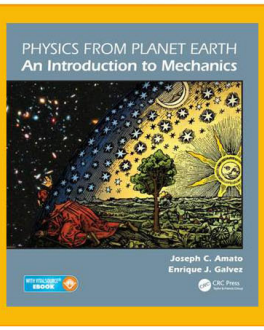

The role of shock waves in expansion tube accelerators

G. Olson, R. Peterson, B. Pulford, M. Seaberg, K. Stein, C. Stelter, and R. Weber
Department of Physics, Bethel University, St. Paul, Minnesota 55112

(Received 20 June 2006; accepted 22 September 2006)

Simulations are combined with laboratory measurements to show the important role of shock waves in a popular physics demonstration, the "ping pong cannon." The simulation and measurements confirm a developing shock wave that reflects from the end of the closed tube and approaching ball and the eventual formation of a transient localized pressure build-up near the exit tape barrier. This 2 atm burst of pressure peaks within a few microseconds of the ball's arrival, resulting from the combination of near ambient gas density and shock heating to about 1200 K. Pulsed schlieren images beyond the exit confirm the sequence of internally reflected shock waves and the intense, hot air pressure pulse that explosively removes the exit tape just prior to the ball arrival.
[DOI: 10.1119/1.2366737]

I. INTRODUCTION

In the "ping-pong cannon" physics demonstration[1–3] a plastic tube with a loose-fitting ping-pong ball at one end is typically sealed at each end with sealing tape, evacuated to a few Torr, and the tape near the ball end is punctured.[4] The ball accelerates as air expands into the tube and is known to reach speeds near 300 m/s after a distance of 2 m.[1] Earlier work has shown that the exit tape barrier becomes detached before the ball reaches the exit (see Fig. 1). The details of the gas dynamics just prior to the ball's violent exit have been unclear and are fundamental to the physics of the demonstration. More complex, multiple stage gas expansion tubes of this sort are widely used in aerospace education and research for producing very high gas speeds and shock waves,[5] but their use in the acceleration of solid objects is much less common.

The detachment of the tape prior to the exit of the ball is the result of highly nonlinear gas dynamics and shock behavior occurring between the ball and the tape. These processes are initiated when the tape at the ball end of the tube is punctured. The acceleration of the ball induces large amplitude compression waves that travel along the tube ahead of the ball. For isentropic flows, these compressions lead to increases in the local sound speed, which result in a steepening of the compression wave and eventual formation of a shock wave.[6] Flow gradients are high across the formed shock wave, resulting in significant heat transfer and frictional effects. Thus, entropy is not conserved across the shock and the isentropic assumption becomes invalid in the shock region.

The formation of the shock wave and resulting reflections in the expansion tube are depicted qualitatively in Fig. 2. The top of Fig. 2 indicates the initial location of the ball and the initial condition for the pressure surrounding the ball. The remainder of Fig. 2 is a space-time diagram that identifies the position of the ball as it accelerates down the tube, the formation of the compression shock, and the ensuing reflections between the closed right end of the tube and the ball. Four flow states are identified as different regions in Fig. 2: Region A indicates the undisturbed air in the tube ahead of the initial shock front; region B indicates the formation of the shock at the leading edge of the compression wave in front of the ball; region C indicates the propagation and reflections of the developed shock wave; and region D represents the expansion of air behind the accelerating ball.

II. NUMERICAL SIMULATION AND ANIMATION OF SHOT DYNAMICS

To gain a better understanding of what is happening in the expansion tube, a one-dimensional (1D) model has been developed that approximates the physical situation in the tube. The model assumes one-dimensional, inviscid, ideal gas flow, no air flow around the ball, and no energy loss at the closed (taped) exit end of the tube. Although an imperfect approximation to this physical system, simulations based on the model exhibit almost all of the major features observed in the physical measurements that are described in the following sections.

To model the fluid-structure interaction between the gas and the ball, four equations are to be solved simultaneously. The 1D compressible Euler equations govern the fluid dynamics and are comprised of three equations: conservation of mass, conservation of momentum, and conservation of energy. A fourth equation governs the dynamics of the ball. The 1D compressible Euler equations are

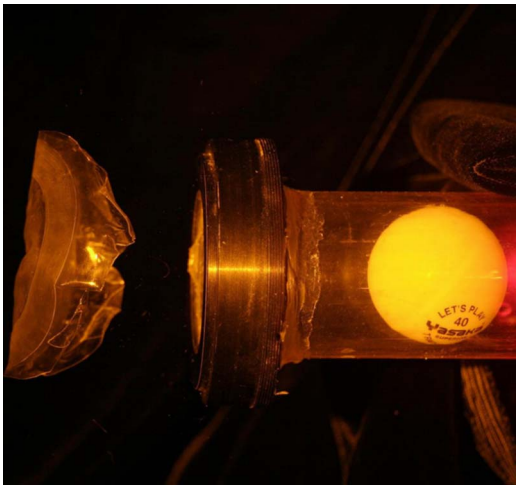

Fig. 1. High speed image of tape removal prior to ball arrival (with 0.4 μs laser illumination) (Ref. 1).

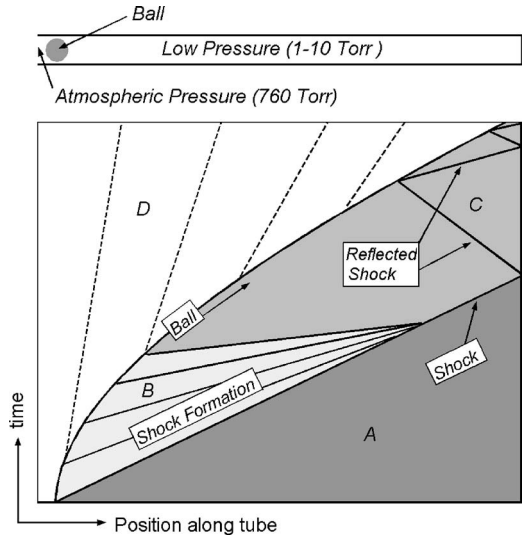

Fig. 2. Shock formation in an expansion tube accelerator in front of an accelerating ball.

$$\frac{\partial \rho}{\partial t} + \frac{\partial (\rho u)}{\partial x} = 0, \tag{1}$$

$$\frac{\partial (\rho u)}{\partial t} + \frac{\partial (\rho u^2 + P)}{\partial x} = 0, \tag{2}$$

$$\frac{\partial (\rho e)}{\partial t} + \frac{\partial (\rho u e + P u)}{\partial x} = 0. \tag{3}$$

Here, ρ is the fluid density, t is the time, u is the fluid velocity along the tube, P is the fluid pressure, and e is the total energy per unit mass. The fluid pressure is related to density, velocity, and energy through an equation of state for ideal gases as

$$P = P(\rho, u, e) = (\gamma - 1)\rho e_i = (\gamma - 1)\rho\left(e - \frac{u^2}{2}\right), \tag{4}$$

where e_i is the internal energy per unit mass and γ is the specific heat ratio of the fluid. The fluid temperature is governed by the ideal gas law[7]

$$T = \frac{e_i}{C_V} = \frac{(\gamma - 1)}{R}\left(e - \frac{u^2}{2}\right), \tag{5}$$

where R is the ideal gas constant and C_V is the specific heat at constant volume.

The equation of motion for the ball from Newton's second law is

$$\frac{\partial U_b}{\partial t} = \frac{(P_l - P_r)}{M_b}\pi R_b^2, \tag{6}$$

where U_b, M_b, and R_b are the velocity, mass, and radius of the ball, respectively. The pressures P_l and P_r act on the left and right sides of the ball. The Euler equations for the fluid and the equation of motion for the ball are coupled by imposing an interface condition, which requires that the velocity of the fluid at the interface is equal to the velocity of the ball, and the pressures to the left and right of the ball are equal to the fluid pressures at the interface.

Numerical solutions for the compressible flow and shock behavior are found using the stabilized space-time finite element formulation.[7,8] This method was introduced in the early 1990s as an interface-tracking technique for the computation of flow problems with moving boundaries and interfaces and is well-suited for handling the motion of the ball within the fluid domain. The method is implemented for the 1D compressible Euler equations using Matlab[9] to carry out simulations on the expansion tube accelerator.

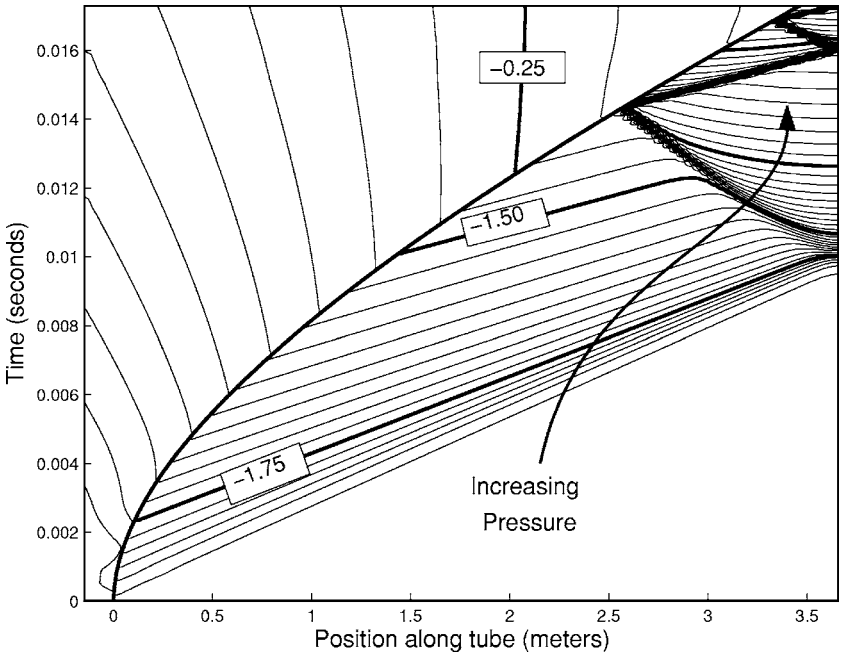

Fig. 3. Contours of constant pressure. Isobars indicate values of $\log_{10}(P/P_{\text{atm}})$ with changes in value of 0.025 between contours, where P_{atm} is standard atmospheric pressure (760 Torr) and is the imposed stagnation pressure at the left boundary.

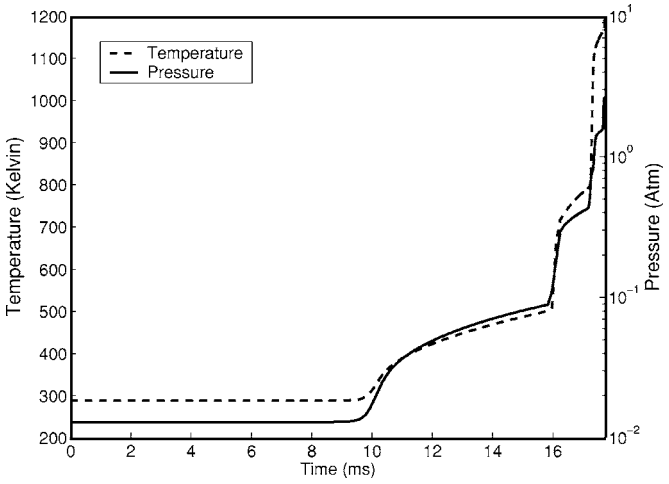

Fig. 4. Predicted temperature and pressure histories. Temperatures correspond to the taped end of the tube, and pressures correspond to a location 4.5 cm from the end of the tube to correlate with subsequent piezoelectric pressure measurements (see Sec. III C).

A simulation of the expansion tube accelerator was carried out using a single-processor desktop computer, with initial air pressure of 10 Torr inside the expansion tube (that is, to the right of the ball) and an atmospheric condition of 760 Torr outside the tube. The ball is initially stationary and the air is initially at rest throughout the entire domain of the fluid. After the simulation is started, the motion of the ball is driven by the air pressure to the left and right of the ball. The fluid solution is governed by the 1D compressible Euler equations [see Eqs. (1)–(3)], with the velocity of the ball imposed as a fluid boundary condition. A converged solution for the coupled compressible fluid and ball dynamics is achieved each time step using an iterative coupling approach. In iterative coupling, individual systems of equations are solved for the dynamics of the ball and the compressible fluid. Coupling is achieved through the transfer of interface information prior to the individual updates. Multiple iterations and transfers of interface information result in a tight coupling between the fluid and the ball dynamics.

The simulation results are highlighted in Figs. 3–5 and predict the shock wave formation and reflections back and forth between the tape and the ball. These reflections occur several times before the ball reaches the end of the tube and a boost in pressure and temperature is triggered with each reflection (see Figs. 3 and 4). Resulting pressures exceeding 2 atm and temperatures exceeding 1200 K are predicted as the ball approaches the taped end of the tube. The peak pressure is surrounded by a high concentration of contours and rapid reflections in the upper right corner of Fig. 3. The high pressure pulse is expected to result in the forceful removal of the tape prior to the ball leaving the end of the tube. The end of the tube experiences a boost in temperature with each reflection, as indicated in Fig. 4.

Unlike the pressure and temperature, which are discontinuous across the ball, the velocity field is continuous (see Fig. 5). This continuity is due to the no-penetration boundary condition that is imposed at the surface of the ball. Maximum velocities of approximately 300 m/s are predicted and are in close agreement with measured values.[1,10]

III. SHOCK MEASUREMENT TECHNIQUES

A. Shock kinematics

The deflection of a He-Ne laser beam by index of refraction gradients allows a determination of the velocities of shock waves present within the tube. As a shock passes through a laser beam (entering through windows along a path perpendicular to the tube axis), the beam will be either deflected further onto or off a small 125 MHz detector depending on the shock's direction, thus producing short voltage

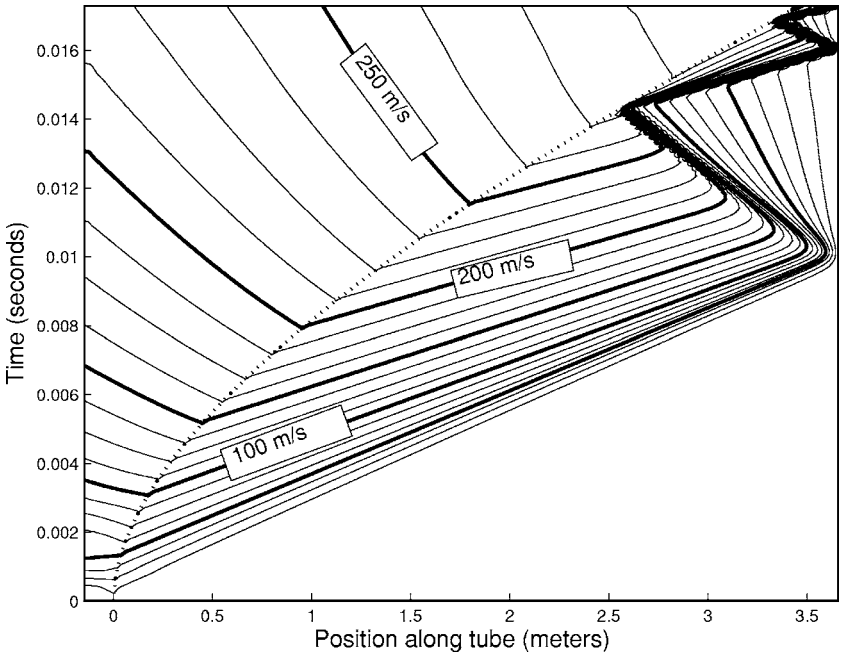

Fig. 5. Contours of constant velocity. Spacing between contours indicates changes in velocity of 12.5 m/s. The dotted line indicates the position of the ball in time.

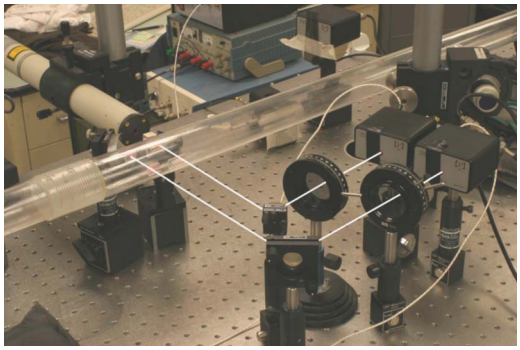

Fig. 6. "Knife edge" shock detection optics, with beam paths added for clarity.

spikes on a recording oscilloscope. Half of the detector's 0.12 mm^2 area is covered with a sharp "knife-edge" of black tape, and the laser beam is initially aligned half on the detector and half on the tape edge to enhance this effect (see Fig. 6). This bending of a 2 mm diameter laser beam due to the strong refractive gradients in the tube is due to the passing shock's step function of increased density. By using a beam splitter, two He-Ne beams (with a 41 mm beam spacing) are moved to multiple locations along the tube to determine the arrival times, directions, and speeds of shocks at these points. When the ball itself passes a beam, a longer voltage pulse is observed, thus providing information on the ball and shock relative positions.

Imploding air (with initial pressures ranging from 1 to 140 Torr) without a ball present led to confirmation of the relation of shock speed to the driver to driven gas pressure. This ratio is given by[5]

$$\frac{P_4}{P_1}=\frac{\gamma-1}{\gamma+1}\left[\frac{2\gamma}{\gamma-1}\mathrm{M}_s^2-1\right]\left[1-\frac{\gamma-1}{\gamma+1}\frac{\mathrm{M}_s^2-1}{\mathrm{M}_s}\right]^{-2\gamma/(\gamma-1)}, \tag{7}$$

where γ is the specific heat ratio (1.4 for air at STP), P_1 is the driven gas pressure (that is, background pressure), P_4 is the driver gas pressure (in our case atmospheric pressure), and M_s is the shock Mach number.[6] When we repeated this

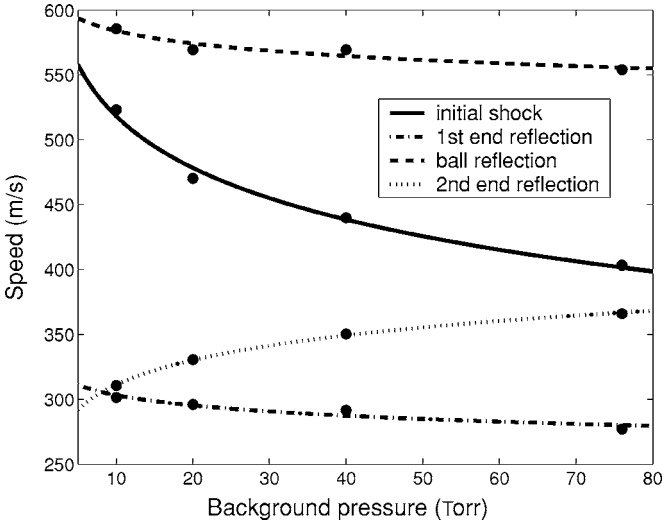

Fig. 7. Shock speeds 25 cm from the end of the tube with the ball.

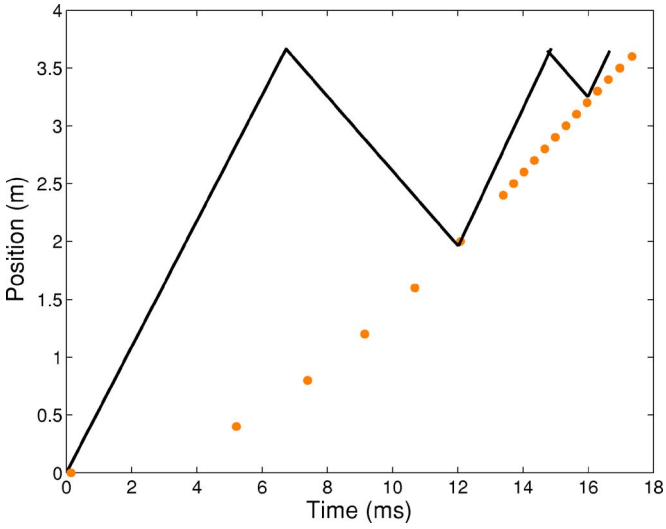

Fig. 8. Linear approximation to position of the shock wave (solid line) and ball (dots) as functions of time. The shock wave positions have been extrapolated from limited data of shock speeds and arrival times at 10 Torr initial background pressure.

experiment while accelerating the ball, the shocks were found to have considerably lower speeds (see Figs. 7 and 8). The lower speeds follow from the interaction between the ball and the shock wave at the onset of a shot. With each successive reflection off the ball, the shock speed grows in magnitude, while after each reflection off the sealed exit end, the shock speed in the lab frame is notably slower.[11] Three distinct forward passages of the shock wave are detected near the exit before the tape is blown off, confirming the simulation's prediction that it is the convergent trapping of the ricocheting shock just prior to the ball's arrival that triggers a rapid pressure and temperature escalation.

The refractive deflection technique has also been used to observe external shocks passing through the tape prior to the exit of the ball. External deflection pulses are observed at times consistent with those found earlier within the tube and fully confirm their 2D imaging with schlieren techniques as shown in Fig. 9.[1]

B. Shock density measurements

Interferometers can monitor changes in the optical path length and provide a quantification of changes of the index of refraction, allowing measurement of both slow and fast variations in the gas density. For example, if the axis of a tube with an inner diameter of 40 mm is oriented perpendicular to one arm of an interferometer, the implosion of air following tape puncture will produce dozens of fringe shifts on a relatively slow time scale (10 ms). A specialized interferometer can also precisely quantify gas density fluctuations on a microsecond time scale such as those produced by the propagation of shock waves along the tube axis. For a given gas, variations in density are largely proportional to the index of refraction, and each fringe shift (2π rad of phase) signals a corresponding change in density. The differential heterodyne interferometer employed in this case can follow changes between two optical paths (0.01λ to several λ) within fractions of microseconds.

The optical system of Fig. 10 facilitates fringe shift measurements by converting the process to one of electronically

Fig. 9. A pulsed schlieren image displays external shock waves beyond the end of the tube (Ref. 1). The convergence of shock waves (centered vertically) has served to remove the tape, and the singular shock wave in the upper half of the image is an earlier shock wave partially reflected internally back toward the ball. Hot air pulses out behind the tape, and the ball is just starting to emerge at the bottom.

measuring the phase shift between two 80 MHz RF signals (where 2π of phase shift corresponds to one wavelength change in the round trip path). The RF signals result from the superposition of optical beams that have been doubly shifted in frequency by a 40 MHz acousto-optic modulator. In the system shown, orthogonal polarizations are separated by a polarizing beam splitter, with each polarization passing through its own arm of the interferometer.[12] One polarization passes through the tube and is impacted by the density changes within the tube, while the other polarization is reflected only by a reference mirror. Lenses before and after the tube focus the radiation near the tube center and minimize the impact of refractive bending due to shocks that can throw the system out of alignment during the measurement.

The radiation of each polarization is reflected back to the laser output mirror. The laser cavity serves as the interferometer "reference arm" for each polarization, thus producing two 80 MHz heterodyne signals from detectors that monitor the orthogonal polarizations present within the zeroth-order beam passed by the acousto-optic modulator. Most table and mount vibrations affect both polarizations in similar ways, thus making phase shifts between these two signals primarily dependent on tube density changes. To obtain the change in phase $\Delta\phi(t)$ between these two signals, a quadrature phase tracking system is used. A RF mixer (and delay line) after

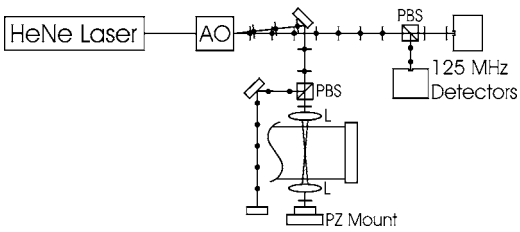

Fig. 10. The interferometry system uses polarizing beamsplitters (PBSs) to produce two beams with orthogonal polarizations. The acousto-optic (AO) cell shifts the first-order beam by 40 MHz each pass, while the zeroth order remains unshifted. One piezoelectric mirror mount is used to allow testing of system response to a prescribed motion.

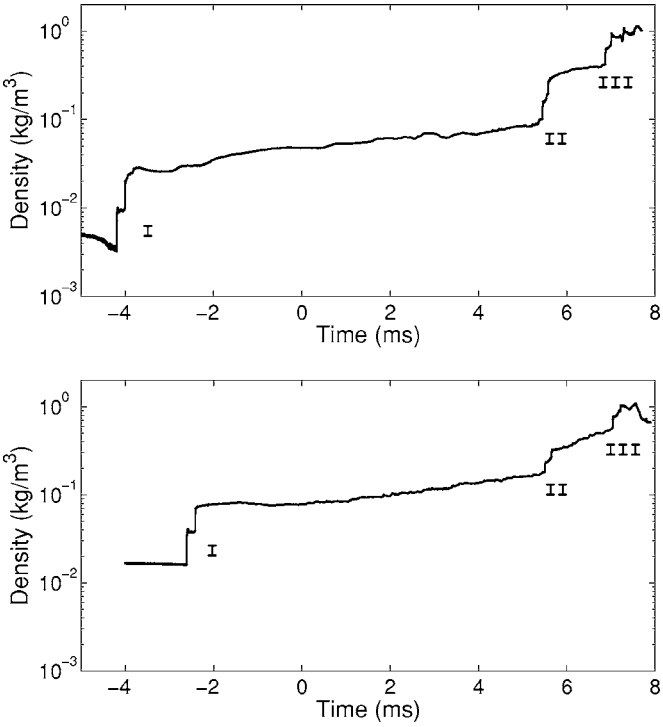

Fig. 11. Logarithmic plot of interferometric results 4.5 cm from the end of the tube at 1 and 10 Torr initial background pressures. All three shocks (I, II, III) are visible.

filtering produces $\sin(\Delta\phi)$ and $\cos(\Delta\phi)$; these signals are digitized with a digital scope (with typically a 10 MHz sampling rate), and a LabView program keeps track of the quadrant of $\Delta\phi$ and plots $\Delta\phi(t)$. For the double pass of the 40 mm inner diameter of the cannon, 240 rad of phase shift are observed for the case of vacuum to atmospheric density, with this calibration facilitating a proportional calculation of the air density in the tube as a function of the time varying phase.

Oscilloscopes are triggered to take density data from a photogate pulse that detects the ball's position in the tube shortly after implosion. Typically several oscilloscopes with varying delays are utilized to each store 10 000 data points for a duration of 1 or 2 ms. LabView compiles these results to allow multiple passages of the shock wave's density change to be measured at a location near the tube exit. The phase may change by as much as 100 rad (0.4 atm) during a few microseconds.

Figure 11 displays the air density on a log scale in the tube 4.5 cm from the exit for two initial "pump down" pressures. Three forward passages of the shock are observed, closely followed in each case by corresponding jumps in the density for the reflected shocks. Even though there is a maximum of the density just prior to the ball's exit, many repeats of these measurements for differing initial pressures still show the density never exceeding that of ambient air density in the room. Thus neither simulation nor measurement suggests a strong, compressive density burst above room ambient air density prior to tape removal at this location.

C. Piezoelectric pressure measurements

A high frequency piezoelectric pressure sensor[13] was employed to directly measure the pressure near the exit end of

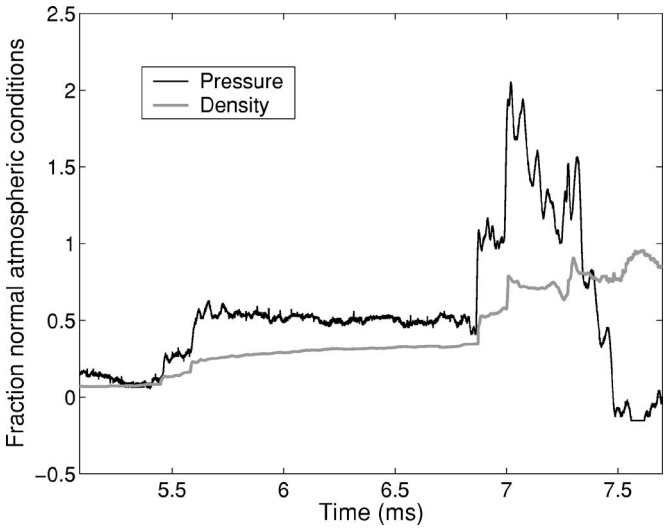

Fig. 12. Plot of data taken at 0.9 Torr initial background pressure at a location 4.5 cm from exit. Both the pressure and density are shown as a fraction of normal atmospheric pressure and density, respectively. The final pressure spike is much more pronounced than the final density, resulting from shock heating. The two-stage pressure jumps at 5.5 and 6.9 ms indicate the advancement and reflection of shocks II and III past the sensor. These pressure jumps are predicted in the numerical simulation as indicated in the final 2 ms of Fig. 4.

the tube. The transducer's voltage versus pressure characteristics are calibrated by a full atmosphere implosion over tens of milliseconds. With the transducer mounted 4.5 cm from the exit tape, pressure shock measurements were recorded for initial background pressures ranging from 0.9 to 20 Torr. Pressure fluctuations due to shocks were found to generally follow the density data at this same location (see Fig. 11) for the earlier passings, but a significant change is observed after the arrival of shock III. The pressure rises to at least 2 atm within several microseconds, while the density elevation is much less pronounced (see Fig. 12). This behavior is consistent with the simulation's prediction of shock heating to nearly 1200 K and a corresponding pressure spike. The time of tape removal is also observed by the sharp drop in pressure shortly after shock III. A photogate positioned just outside the tube also demonstrates synchronization between the tape removal and the internal plunge in pressure. Thus it is clear for this 3.6 m tube that shock III triggers the tape removal by initiating a short pulse of pressure and temperature.

The schlieren images of shock wave fronts passing through the tape (see Fig. 9) were produced in a different PVC cannon of length 2.9 m. The pressure sensor was transferred to this tube to determine if the shock waves behaved similarly to those of the 3.6 m tube. In the shorter tube the fourth incident shock wave (rather than the third) is found to produce the tape removal conditions because the shocks now have a shorter path to travel as they reflect off the tape and ball. In this case it is therefore shocks III and IV that are imaged in the pulsed schlieren image external to the tube.[1]

IV. CONCLUSION

A 1D model of implosive nonlinear gas dynamics and high speed optical measurements of the "ping-pong cannon" combine to reveal a complex but reproducible sequence of events within the cannon. Only by simultaneous measurements of both densities and pressures has it been possible to properly test many predictions of the simulation, including the focusing of shock energy to produce a shock-heated, barrier-removing explosive event just prior to the exit of the ball. The simulation and measurements provide a very consistent description for shock wave development and the eventual formation of the localized pressure build-up near the exit tape barrier. The predicted shock magnitudes and speeds are in close agreement with measurements. Although measurements indicate the immediate presence of a highly developed shock wave, the simulation indicates a smoother build up of shock properties. These minor discrepancies are likely due to assumptions in the model, such as no air flow around the ball and rigid body treatment of the ball. One of the most rewarding aspects of this combined experimental and numerical physics effort has been to gain a much fuller understanding of the striking pulsed schlieren image of Fig. 9.

ACKNOWLEDGMENTS

Generous support for this undergraduate student and faculty effort has come from the NASA Minnesota Space Grant and the Carlsen-Lewis Physics Endowment at Bethel University. We are especially grateful to Jon Barber, Jack Netland, and Hank Ryan of Minnesota's Physics Force for helping with our design of quality cannons and their insightful questions about "how this thing really works." Tom Greenlee and the referees have made valuable suggestions leading to the final version of this paper.

[1] R. Peterson, B. Pulford, and K. Stein, "The ping-pong cannon: A closer look," Phys. Teach. **43**(1), 22–25 (2005).
[2] J. Cockman, "Improved vacuum bazooka," Phys. Teach. **41**(4), 246–247 (2003).
[3] E. Ayars and L. Buchholtz, "Analysis of the vacuum cannon," Am. J. Phys. **72**(7), 961–963 (2004).
[4] The acrylic tube used for much of the study was 3.6 m long with an inner diameter of 42 mm. The balls were typically 39.4 mm in diameter with a mass of 2.4 g. The initial pressures were varied from 0.7 Torr up to as high as 76 Torr. Similar results were obtained for a 2.9 m PVC tube of about 40 mm inner diameter.
[5] H. McMahon, J. Jagoda, N. Komerath, and J. Seitzman, "Transient measurements in a shock tube," Lab manual, Georgia Tech School of Aerospace Engineering (2005), ⟨www.ae.gatech.edu/classes/ae3051/AE3051Labshocktube.pdf⟩.
[6] H. W. Liepmann and A. Roshko, *Elements of Gas Dynamics* (Wiley, New York, 1957), pp. 39–81.
[7] S. Aliabadi and T. Tezduyar, "Space-time finite element computation of compressible flows involving moving boundaries and interfaces," Comput. Methods Appl. Mech. Eng. **43**, 209–223 (1993).
[8] T. Tezduyar, "Stabilized finite element formulations for incompressible flow computations," Adv. Appl. Mech. **28**, 1–44 (1992).
[9] Matlab, Version 6.5.0, Release 13.
[10] See EPAPS Document No. E-AJPIAS-74-020612 for additional color figures and animation. These figures and animations are also at ⟨www.bethel.edu/~kstein/ShockTube/main.html⟩. This document can be reached via a direct link in the online article's HTML reference section or via the EPAPS homepage (www.aip.org/pubservs/epaps.html).
[11] The shock now moves in opposition to the background velocity of gas driven by the earlier "downstream" passage.
[12] T. Carlson, R. Groschen, S. Denzer, T. Greenlee, R. Peterson, and G. Robinson, "Vibration resistant direct-phase detecting optical interferometers," Appl. Opt. **36**(28), 7162–7171 (1997).
[13] The Piezotronics Model 113A21 Dynamic Pressure Sensor is designed for detecting high frequency pressure phenomena and is well-suited for shock tube analysis.